



ORIGINAL ARTICLE

Jia Kang · Long-Xu Tan · Quan-Pu Liu · Si-Yu Wang ·  
Otto T. Bruhns · Heng Xiao

# Unified and accurate simulation for large elastic strain responses of rubberlike soft materials under multiple modes of loading

Received: 13 July 2023 / Accepted: 12 October 2023 / Published online: 17 November 2023  
© The Author(s) 2023

**Abstract** A new and explicit form of the multi-axial elastic potential for elastic soft materials is constructed by means of two invariants of the Hencky strain. The new elasticity model with this form can bypass coupling complexities and uncertainties usually involved in parameter identification. Namely, exact closed-form solutions of decoupled nature are obtainable for stress responses under multiple benchmark modes. Unlike usual solutions with numerous coupled parameters, such new solutions are independent of one another and, as such, data sets for multiple benchmark modes can be separately matched with mutually independent single-variable functions. A comparative study is presented between a few well-known models and the new model. Results show that predictions from the former agree well with uniaxial and biaxial data, as known in the literature, but would be at variance with data for the constrained stress response in the plane-strain extension. In contrast, predictions from the new model agree accurately with all data sets. Furthermore, exact solutions for the Poynting effect of freely twisted elastic thin-walled tube are obtained from the new model.

**Keywords** Soft materials · Elastic potential · Multiple modes · Exact solutions · Decoupled approach

---

Communicated by Andreas Öchsner.

---

J. Kang · L.-X. Tan · Q.-P. Liu · S.-Y. Wang (✉) · H. Xiao (✉)  
School of Mechanics and Construction Engineering and MOE Key Lab of Disaster Forecast and Control in Engineering,  
Jinan University, Guangzhou 510632, China  
E-mail: siyu0904@foxmail.com

J. Kang  
E-mail: wanghy2020jnu@163.com

L.-X. Tan  
E-mail: 17328320692@163.com

Q.-P. Liu  
E-mail: yunyachenx@163.com

H. Xiao  
E-mail: xiaoheng@shu.edu.cn

O. T. Bruhns (✉)  
Institute of Mechanics, Ruhr-University Bochum, Bochum 44780, Germany  
E-mail: otto.bruhns@rub.de

## 1 Introduction

Various elastic soft materials serve as constituent materials of artificial and natural structures (cf., e.g., [1]). Examples for such materials include rubbers, polymer gels, and biological soft tissues, e.g., skins, arteries and blood vessels, etc. Large elastic strain responses of such soft materials are simulated based on the elastic potential representing the strain energy. According to the standard procedures in continuum thermodynamics, each specific form of the latter establishes a hyperelastic constitutive model which specifies the stress response to each finite strain. A reasonable model should be such that its predictions under multiple modes of loading agree simultaneously with test data for these modes. Usually, a few benchmark modes are taken into consideration, including the uniaxial extension and compression of a bar, the equi-biaxial extension of a plate, the plane-strain extension and compression of a strip, etc.

Earlier, simple forms of the elastic potential were presented, such as the Hencky model [2,3], the neo-Hookean model [4], and the Mooney–Rivlin model [4]. Such simple models would be limited to a moderate deformation range. Later, various advanced models were established toward matching large strain data for benchmark deformation modes, such as the Ogden model [5], the Arruda–Boyce model [6], and the Gent model [7,8], to name but a few. Of them, the latter two with only two adjustable parameters<sup>1</sup> stand out in the sense that their predictions can not only match large strain data for uniaxial extension and plane-strain extension but can approximately match equi-biaxial extension data. On the other side, the Ogden model with six parameters can well match large strain data for all three benchmark modes. However, it appears that applicability of these models still need to be examined even for the plane-strain extension mode. In fact, good agreement can be achieved with the stress data in the loading direction, but that would not be the case for the stress data in the constrained direction, as will be evidenced in a comparative study here.

In addition to the benchmark modes in the foregoing, large free torsion of thin-walled tubes under twisting loads are noticeable with the well-known Poynting effect [10]. In fact, a freely twisted elastic tube with finite torsion angle will display recoverable changes in the axial length and the wall thickness as well as the averaged radius. Such noticeable finite strain effects need to be studied particularly for thin-walled tubes made of soft materials such as polymer gels and biological soft tissues including arteries and blood vessels, etc. Simulation results with certain simple models may be found, e.g., in Zubov [11], De Pascalis et al. [12], Zubov and Sheidakov [13], Mihai and Goriely [14], Merodio and Ogden [15], Anssari-Benam and Horgan [16], and Zingerman et al. [17]. In particular, reference may be made to recent results for torsional behaviors of biological soft tissues in Balbi et al. [18] and Horgan and Murphy [19].

Since the Poynting effect for elastic soft tubes may be much appreciable up to very large deformations, objectives in two respects need to be achieved for an accurate analysis. On the one hand, a new elastic constitutive model should be established toward accurately matching all large strain data for the benchmark modes, and exact results for the Poynting effect can be derived from this new model, on the other hand.

Toward the above objectives, a new form of the elastic potential will be constructed by means of two well-designed invariants of Hencky's logarithmic strain. The hyper-elastic constitutive model with this new form can bypass coupling complexities and uncertainties involved in identifying a set of coupling adjustable parameters. Namely, exact solutions of decoupled nature are obtainable for stress responses under multiple benchmark modes. Unlike usual solutions with an inextricably coupled set of adjustable parameters, such new solutions are independent of one another and, as such, multiple data sets for the foregoing benchmark modes can be separately matched with mutually independent single-variable functions. A comparative study will be presented between a few well-known models and the new model. It will be shown that predictions from the former agree well with uniaxial and biaxial data, as known in literature, but would be at variance with data for the constrained stress response in the plane-strain extension. In contrast, predictions from the new model can agree well with all data sets. Furthermore, with a new technique of treating nonlinear coupling equations in a most recent study [20], exact solutions for the large torsion of a thin-walled tube with free ends will be obtained from the new model.

## 2 New model with new elastic potential

In this section, a new form of the elastic potential will be constructed for the purpose of matching multiple data sets for the benchmark modes. Results will be derived based upon Hencky's logarithmic strain [2,3]. Details

<sup>1</sup> See also a latest development [9] in this respect.

for noticeable features of the Hencky strain may be found, e.g., in Hill [21], Anand [22], and Fitzgerald [23]. Reference may also be made to a survey article [24].

## 2.1 Hencky invariants

Let  $\mathbf{B} = \mathbf{F} \cdot \mathbf{F}^T$  be the left Cauchy–Green tensor with the deformation gradient  $\mathbf{F}$  and, moreover, let  $\chi_s = \lambda_s^2$  and  $\mathbf{B}_s$  be the three eigenvalues and the corresponding eigenprojections of  $\mathbf{B}$ , respectively. Hencky's logarithmic strain tensor is designated by  $\mathbf{h}$  and given by

$$\mathbf{h} = \frac{1}{2} \ln \mathbf{B} = \frac{1}{2} \sum_{s=1}^3 (\ln \chi_s) \mathbf{B}_s. \quad (1)$$

The three basic invariants of the Hencky strain are as follows:

$$i_s = \text{tr} \mathbf{h}^s = \ln^s \lambda_1 + \ln^s \lambda_2 + \ln^s \lambda_3, \quad s = 1, 2, 3. \quad (2)$$

The volumetric ratio  $J$  is given by

$$J = \det \mathbf{F} = \lambda_1 \lambda_2 \lambda_3.$$

The incompressibility condition  $J = 1$  is equivalent to

$$i_1 = \text{tr} \mathbf{h} = 0. \quad (3)$$

In this case, the Hencky strain  $\mathbf{h}$  and its deviatoric part

$$\tilde{\mathbf{h}} = \mathbf{h} - \frac{1}{3} i_1 \mathbf{I}$$

are equal to each other, i.e.,

$$\mathbf{h} = \tilde{\mathbf{h}}. \quad (4)$$

Hence, the three basic invariants of the deviatoric Hencky strain are as follows:

$$j_1 = \text{tr} \tilde{\mathbf{h}} = 0,$$

$$j_2 = \text{tr} \tilde{\mathbf{h}}^2 = \ln^2 \lambda_1 + \ln^2 \lambda_2 + \ln^2 \lambda_3, \quad (5)$$

$$j_3 = \text{tr} \tilde{\mathbf{h}}^3 = \ln^3 \lambda_1 + \ln^3 \lambda_2 + \ln^3 \lambda_3. \quad (6)$$

The constitutive equation of an isotropic, incompressible hyper-elastic solid is expressible as the following direct potential relation [21,23]:

$$\boldsymbol{\sigma} = \frac{\partial W}{\partial \mathbf{h}} + p \mathbf{I}. \quad (7)$$

In the above,  $p$  is the indeterminate averaged part of the Cauchy stress  $\boldsymbol{\sigma}$ ,  $\mathbf{I}$  is the identity tensor and the elastic potential  $W$  is a scalar function of the Hencky strain, i.e.,

$$W = W(\mathbf{h}). \quad (8)$$

The isotropy condition requires that the above elastic potential be represented by a function of the two basic invariants  $j_2$  and  $j_3$  and, generally, a function of any other two equivalent Hencky invariants. For our purpose, it will be essential to use two well-designed Hencky invariants, designated by  $\psi$  and  $\gamma$  and given by (cf., e.g., [25])

$$\psi = \sqrt{\frac{2}{3}} j_2, \quad (9)$$

$$\gamma = \sqrt{6} \frac{j_3}{j_2^{1.5}}. \quad (10)$$

It is worth pointing out that similar forms of the mode invariant  $\gamma$  were used in describing finite elastic strains earlier in Novozhilov [26] and in formulating strength criteria in the stress space recently in Kolupaev [27] and Altenbach and Kolupaev [28].

With certain favorable properties, the two Hencky invariants  $\varphi$  and  $\gamma$  in Eqs. (9, 10) are introduced to characterize the magnitude and the mode of the Hencky strain, respectively. In particular,  $\varphi$  and  $-\varphi$  just provide the axial Hencky strain for the uniaxial extension mode and the uniaxial compression mode, respectively. Moreover, the mode invariant  $\gamma$  yields the values 1, -1, 0 for uniaxial extension and compression and plane-strain extension, respectively. Namely,

$$\varphi = \begin{cases} +\ln \lambda & \text{for uniaxial extension,} \\ -\ln \lambda & \text{for uniaxial compression,} \end{cases} \quad (11)$$

and

$$\gamma = \begin{cases} +1 & \text{for uniaxial extension,} \\ -1 & \text{for uniaxial compression,} \\ 0 & \text{for plane-strain extension,} \end{cases} \quad (12)$$

where  $\lambda$  is the axial stretch ratio for an axially loaded bar. Generally,

$$-1 \leq \gamma \leq +1. \quad (13)$$

Details may be found in [25].

## 2.2 New elastic potential

As indicated before, the elastic potential of an isotropic, incompressible highly elastic material is expressible as follows:

$$W = W(\varphi, \gamma). \quad (14)$$

Given a form of the potential  $W$ , the hyperelastic stress–strain relation Eq. (7) may be given in the form (cf. [25], Eq. (79)):

$$\boldsymbol{\sigma} = \left[ \frac{2}{3} \varphi^{-1} \frac{\partial W}{\partial \varphi} \mathbf{h} + 2\varphi^{-3} \frac{\partial W}{\partial \gamma} (2\mathbf{h}^2 - \gamma\varphi\mathbf{h} - \varphi^2\mathbf{I}) \right] + p\mathbf{I}. \quad (15)$$

Now we construct a new and explicit form of the elastic potential  $W$  by means of the Hencky invariants  $\varphi$  and  $\gamma$  in Eqs. (9, 10). The main idea is explained as follows. For the three benchmark modes including the uniaxial extension and compression as well as the plane-strain extension, it is deduced from Eq. (12) that the elastic potential Eq. (14) reduces to three single-variable functions of the magnitude invariant  $\varphi$ . The latter three just supply the strain energies for the three modes at issue. Moreover, the value of the derivative  $\partial W/\partial \gamma$  at  $\gamma = 0$  (i.e., plane-strain extension) just prescribes the stress response in the constrained direction. Thus, a cubic polynomial form of the elastic potential in  $\gamma$  may be constructed, so that the strain energies for the three benchmark modes with  $\gamma = \pm 1, 0$  as well as the constrained stress response for the plane-strain extension with  $\gamma = 0$  can be automatically reproduced. Such a new form of the elastic potential is as follows:

$$W = \psi_3(\varphi)\gamma^3 + \psi_2(\varphi)\gamma^2 + \psi_1(\varphi)\gamma + \psi_0(\varphi) \quad (16)$$

with

$$\psi_0(\varphi) = w_p(\sqrt{0.75}\varphi), \quad (17)$$

$$\psi_1(\varphi) = \frac{1}{6}\varphi \left[ g_p(\sqrt{0.75}\varphi) - 2\bar{g}_p(\sqrt{0.75}\varphi) \right], \quad (18)$$

$$\psi_2(\varphi) = \frac{1}{2}w_t(\varphi) + \frac{1}{2}w_c(-\varphi) - w_p(\sqrt{0.75}\varphi), \quad (19)$$

$$\psi_3(\varphi) = \frac{1}{2}w_t(\varphi) - \frac{1}{2}w_c(-\varphi) - \frac{1}{6}\varphi \left[ g_p(\sqrt{0.75}\varphi) - 2\bar{g}_p(\sqrt{0.75}\varphi) \right], \quad (20)$$

and

$$w_t(h) = \int_0^h f_t(h)dh, \quad h \geq 0, \quad (21)$$

$$w_c(h) = \int_0^h f_c(h)dh, \quad h \leq 0, \quad (22)$$

$$w_p(h) = \int_0^h g_p(h)dh, \quad h \geq 0. \quad (23)$$

As will be seen slightly later, the  $h$  in Eqs. (21, 22) is the axial Hencky strain for an axially loaded bar, while the  $h$  in Eq. (23) is the Hencky strain in the loading direction for the plane-strain extension of a strip. Moreover, the  $f_t(h)$  and  $f_c(h)$  are two single-variable functions representing the axial stress responses in uniaxial tension and compression, respectively, while the  $g_p(h)$  and  $\bar{g}_p(h)$  are two single-variable functions characterizing the plane-strain stress responses in the loading and the constrained direction, respectively. Their forms may be independently chosen in matching test data for the three benchmark modes. Details will be given in the next section.

Results in Eqs. (16)–(23) represent a development of the previous study [20,25,29–32]. Here, a new form is presented with the uniaxial strain energies Eqs. (21, 22) in a broader sense.

### 3 Exact solutions of decoupled nature

In this section, exact solutions will be presented to the stress responses for the three benchmark modes and the decoupled nature of them will be explained.

#### 3.1 Uniaxial extension and compression

First, an axially loaded bar is treated. Let  $\mathbf{e}$  be a unit vector in the axial direction and let  $\sigma$  and  $\lambda$  be the axial Cauchy stress and the axial stretch ratio, respectively. The Cauchy stress tensor and the deformation gradient as well as the Hencky strain are of the forms:

$$\boldsymbol{\sigma} = \sigma \mathbf{e} \otimes \mathbf{e}, \quad \mathbf{F} = \lambda \mathbf{e} \otimes \mathbf{e} + \lambda^{-0.5}(\mathbf{I} - \mathbf{e} \otimes \mathbf{e}), \quad \mathbf{h} = h \mathbf{e} \otimes \mathbf{e} - 0.5h(\mathbf{I} - \mathbf{e} \otimes \mathbf{e}), \quad (24)$$

with the axial Hencky strain  $h = \ln \lambda$ . Then, by using Eqs. (11, 12) and Eqs. (15)–(23) the following results are deduced:

$$\begin{cases} \sigma = f_t(h) & \text{for } h \geq 0, \\ \sigma = f_c(h) & \text{for } h \leq 0. \end{cases} \quad (25)$$

It turns out that the two single-variable functions  $f_t(h)$  and  $f_c(h)$  in Eqs. (21, 22) just supply the axial Cauchy stress responses in tension and compression, respectively, and, accordingly, Eqs. (21, 22) are just the uniaxial strain energies in tension and compression.

#### 3.2 Plane-strain extension

Next, the plane-strain extension of a plate strip is taken into consideration. Let  $\mathbf{e}$ ,  $\bar{\mathbf{e}}$  and  $\mathbf{a}$  be three orthonormal vectors in the loading, the constrained and the unconstrained direction, respectively, and let  $\sigma_p$  and  $\bar{\sigma}_p$  be the normal stresses in the loading and the constrained direction. Then, the Cauchy stress tensor, the deformation gradient and the Hencky strain are of the forms:

$$\boldsymbol{\sigma} = \sigma_p \mathbf{e} \otimes \mathbf{e} + \bar{\sigma}_p \bar{\mathbf{e}} \otimes \bar{\mathbf{e}}, \quad \mathbf{F} = \lambda \mathbf{e} \otimes \mathbf{e} + \lambda^{-1} \mathbf{a} \otimes \mathbf{a}, \quad \mathbf{h} = h(\mathbf{e} \otimes \mathbf{e} - \mathbf{a} \otimes \mathbf{a}), \quad (26)$$

where  $\lambda \geq 1$  and  $h = \ln \lambda \geq 0$  are the extension ratio and the Hencky strain in the loading direction.

Again, by using Eqs. (15–23) with

$$\gamma = 0, \quad \varphi = \sqrt{\frac{4}{3}}h,$$

the results below are derived:

$$\begin{cases} \sigma_p = g_p(h), \\ \bar{\sigma}_p = \bar{g}_p(h). \end{cases} \quad (27)$$

It turns out that the two single-variable functions  $g_p(\cdot)$  and  $\bar{g}_p(\cdot)$  in the elastic potential in Eqs. (16)–(23) prescribe the stress responses in the loading and the constrained direction and, besides, Eq. (23) supplies the strain energy for the plane-strain extension.

### 3.3 Coupled versus decoupled

A number of unknown parameters are introduced in various known models. Coupling complexities and uncertainties should be treated in fitting benchmark test data for the uniaxial, bi-axial and plane-strain extension modes, as exemplified below with the Ogden model.

The three-term Ogden potential is of the form:

$$W_O = \sum_{i=1}^3 \frac{\mu_i}{\alpha_i} (\lambda_1^{\alpha_i} + \lambda_2^{\alpha_i} + \lambda_3^{\alpha_i} - 3), \quad (28)$$

where the  $\lambda_r$  are the principal stretches and the  $(\mu_i, \alpha_i)$  are six unknown parameters that are coupled with one another in fitting test data for the three benchmark modes, as explained below.

First, for the uniaxial extension and compression as specified by Eq. (24), the axial stress response is given by

$$\sigma = \lambda_1 \frac{\partial W_O}{\partial \lambda_1} - \lambda_2 \frac{\partial W_O}{\partial \lambda_2}, \quad (29)$$

where

$$\lambda_1 = \lambda, \quad \lambda_2 = \lambda_3 = \lambda^{-0.5}.$$

Next, for the plane-strain extension as specified by Eq. (26), the stress responses in the loading and the constrained direction are prescribed by

$$\begin{cases} \sigma_p = \lambda_1 \frac{\partial W_O}{\partial \lambda_1} - \lambda_3 \frac{\partial W_O}{\partial \lambda_3}, \\ \bar{\sigma}_p = \lambda_2 \frac{\partial W_O}{\partial \lambda_2} - \lambda_3 \frac{\partial W_O}{\partial \lambda_3}, \end{cases} \quad (30)$$

where

$$\lambda_1 = \lambda, \quad \lambda_2 = 1, \quad \lambda_3 = \lambda^{-1}.$$

It may be evident that the responses in Eqs. (29, 30) are inextricably coupled with one another in fitting the six unknown parameters  $\mu_i$  and  $\alpha_i$  to test data for the three benchmark modes.

As contrasted with the above coupling complexity, the stress responses Eqs. (25, 27) derived from the new model are of decoupled nature. Namely, the four single-variable functions therein may be independently chosen to separately match test data for the three benchmark modes. Such single-variable functions can further be presented in explicit forms, as shown below.

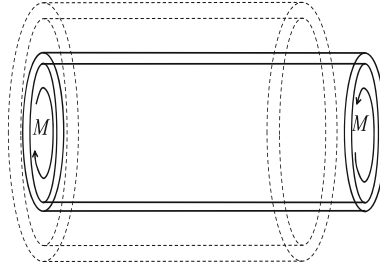


**Fig. 1** Freely twisted thin-walled tube subjected to twisting moment  $M$

### 3.4 Stress–strain functions in explicit forms

The uniaxial tensile and compressive stress–strain functions in Eq. (25) may be given by a rational function in a uniform form (cf., e.g., [25, 29]):

$$\sigma = f(h) = E(1 - \alpha)h + \frac{E\alpha h}{\left(1 - \frac{h}{h_t}\right)\left(1 + \frac{h}{h_c}\right)} \quad (31)$$

with

$$\sigma_t = f(h), \quad h \geq 0, \quad (32)$$

$$\sigma_c = f(h), \quad h \leq 0. \quad (33)$$

In Eq. (31),  $E$  is Young's modulus at the infinitesimal strain,  $\alpha > 0$  is a dimensionless parameter, and the  $h_t > 0$  and  $h_c > 0$  are referred to as the extension limit and the compression limit characterizing the strain-stiffening effects in extension and compression, respectively.

On the other side, for the plane-strain extension, the stress–strain function in Eq. (27) for the stress response in the loading direction is given as follows:

$$\sigma_p = \frac{4}{3}Eh \left( 1 - \alpha_p + \frac{\alpha_p}{1 - \frac{h^2}{h_p^2}} \right), \quad (34)$$

while the stress–strain function in Eq. (27) for the constrained stress response by

$$\bar{\sigma}_p = \frac{2}{3}Eh \left( 1 - \bar{\alpha}_p + \frac{\bar{\alpha}_p}{1 - \frac{h^2}{\bar{h}_p^2}} \right). \quad (35)$$

In the above, the two parameter pairs  $(\alpha_p, h_p)$  and  $(\bar{\alpha}_p, \bar{h}_p)$  characterize the stress responses in the loading and the constrained direction, respectively.

## 4 Exact analysis for large free torsion

Let  $r_0$  and  $t_0$  be the initial average radius and the wall thickness of a thin-walled cylindrical tube, respectively. Large free torsion of a tube subjected to the twisting moment  $M$  is schematically shown in Fig. 1. Each cross section of a freely twisted tube will be rotated about the symmetry axis of the tube through an angle and changes will be expected in the length, the averaged radius and the wall thickness. Details are given below (cf., e.g., [20]).

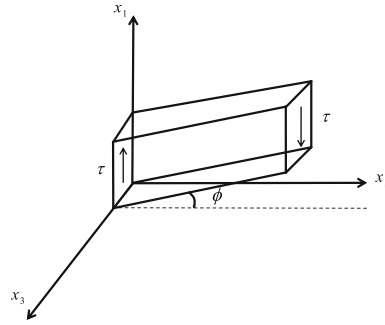


**Fig. 2** Pure shear of a rectangular plate element

#### 4.1 Kinematics

The torsion angle per unit current length is denoted as  $\phi$  and the ratios of the current average radius, axial length and wall-thickness to their undeformed counterparts are designated by  $\xi_1$ ,  $\xi_2$  and  $\xi_3$ , respectively. Moreover, the shear stress on each cross section is uniform and signified by  $\tau$ .

The deformation state of the free-twisted tube can be described by the deformation of a rectangular thin plate element embedded, with the plate sides in the axial and circumferential directions of the tube. Such a plate element experiences pure shear deformation, as depicted in Fig. 2. With  $X_i$  and  $x_i$  the initial and current Cartesian coordinates of this plate element, the deformation of such a plate element may be prescribed as follows:

$$x_1 = \xi_1 X_1 + \omega X_2, \quad x_2 = \xi_2 X_2, \quad x_3 = \xi_3 X_3. \quad (36)$$

In the above, the  $\omega$  is known as the shear amount given by

$$\omega = \xi_2 \tan \phi. \quad (37)$$

Then, the deformation gradient and the left Cauchy–Green tensor are given by

$$\mathbf{F} = \frac{\partial x_i}{\partial X_j} \mathbf{e}_i \otimes \mathbf{e}_j = \xi_1 \mathbf{e}_1 \otimes \mathbf{e}_1 + \xi_2 \mathbf{e}_2 \otimes \mathbf{e}_2 + \xi_3 \mathbf{e}_3 \otimes \mathbf{e}_3 + \omega \mathbf{e}_1 \otimes \mathbf{e}_2, \quad (38)$$

$$\mathbf{B} = (\xi_1^2 + \omega^2) \mathbf{e}_1 \otimes \mathbf{e}_1 + \xi_2^2 \mathbf{e}_2 \otimes \mathbf{e}_2 + \xi_3^2 \mathbf{e}_3 \otimes \mathbf{e}_3 + \omega \xi_2 (\mathbf{e}_1 \otimes \mathbf{e}_2 + \mathbf{e}_2 \otimes \mathbf{e}_1). \quad (39)$$

The incompressibility condition yields:

$$\xi_1 \xi_2 \xi_3 = 1. \quad (40)$$

On the other side, the stress tensor is as follows:

$$\boldsymbol{\sigma} = \tau (\mathbf{e}_1 \otimes \mathbf{e}_2 + \mathbf{e}_2 \otimes \mathbf{e}_1). \quad (41)$$

The current average radius and thickness  $r$  and  $t$  are given by

$$r = \xi_1 r_0, \quad t = \xi_3 t_0, \quad (42)$$

and hence the twisting moment  $M$  by

$$M = (2\pi r t \tau) \cdot r = 2\pi r_0^2 t_0 \xi_1^2 \xi_3 \tau. \quad (43)$$

For future use, the three eigenvalues of the left Cauchy–Green tensor  $\mathbf{B}$  are given by:

$$\begin{cases} \chi_1 = \lambda_1^2 = \left( \frac{1}{2} \left( \sqrt{(\xi_1 + \xi_2)^2 + \omega^2} + \sqrt{(\xi_1 - \xi_2)^2 + \omega^2} \right) \right)^2, \\ \chi_2 = \lambda_2^2 = \left( \frac{1}{2} \left( \sqrt{(\xi_1 + \xi_2)^2 + \omega^2} - \sqrt{(\xi_1 - \xi_2)^2 + \omega^2} \right) \right)^2, \\ \chi_3 = \lambda_3^2 = (\xi_1 \xi_2)^{-2}, \end{cases} \quad (44)$$



and the three corresponding eigenprojections of  $\mathbf{B}$  by

$$\mathbf{B}_1 = \frac{\bar{\mathbf{B}} - \chi_2 \bar{\mathbf{I}}}{\chi_1 - \chi_2}, \quad \mathbf{B}_2 = \frac{\bar{\mathbf{B}} - \chi_1 \bar{\mathbf{I}}}{\chi_2 - \chi_1}, \quad \mathbf{B}_3 = \mathbf{e}_3 \otimes \mathbf{e}_3, \quad (45)$$

where

$$\bar{\mathbf{B}} = \mathbf{B} - (\xi_1 \xi_2)^{-2} \mathbf{e}_3 \otimes \mathbf{e}_3, \quad (46)$$

$$\bar{\mathbf{I}} = \mathbf{I} - \mathbf{e}_3 \otimes \mathbf{e}_3. \quad (47)$$

Hence,

$$\mathbf{h}^s = (\ln^s \lambda_1) \mathbf{B}_1 + (\ln^s \lambda_2) \mathbf{B}_2 + (\ln^s \lambda_3) \mathbf{B}_3, \quad s = 1, 2. \quad (48)$$

#### 4.2 Exact solutions

Let the content in the square brackets at the right-hand side of Eq. (15), i.e., the gradient  $\partial W / \partial \mathbf{h}$ , be designated by  $\mathbf{A}$ . By using Eq. (40), it may be inferred that each non-vanishing component  $A_{ij}$  is a function of  $\xi_1$ ,  $\xi_2$  and  $\omega$ . From this and Eqs. (15, 41), the governing equation may be derived as follows:

$$\begin{cases} A_{11}(\xi_1, \xi_2, \omega) + p = 0, \\ A_{22}(\xi_1, \xi_2, \omega) + p = 0, \\ A_{33}(\xi_1, \xi_2, \omega) + p = 0, \\ A_{12}(\xi_1, \xi_2, \omega) = \tau. \end{cases} \quad (49)$$

In the above, expressions for the four non-vanishing components  $A_{ij}$  are obtained by using Eqs. (44)–(48) and given as follows [20]:

$$\begin{cases} A_{11} = \frac{1}{3} \psi^{-1} (z_1 + z_2) \frac{\partial W}{\partial \psi} - \sqrt{1.5} j_2^{-2.5} (z_1 - z_2)^2 (j_2 + 3z_1 z_2) \frac{\partial W}{\partial \gamma}, \\ A_{12} = (z_1 - z_2) \left( \frac{1}{3} \psi^{-1} \frac{\partial W}{\partial \psi} + 3\sqrt{1.5} j_2^{-2.5} (z_1 + z_2) (j_2 + 3z_1 z_2) \frac{\partial W}{\partial \gamma} \right), \\ A_{22} = A_{11}, \quad A_{33} = -2A_{11}, \end{cases} \quad (50)$$

with

$$z_1 = 0.5 \ln \chi_1, \quad z_2 = 0.5 \ln \chi_2, \quad j_2 = 2z_1^2 + 2z_2^2 + 2z_1 z_2, \quad j_3 = -3z_1^2 z_2 - 3z_1 z_2^2. \quad (51)$$

Toward working out solutions for  $\xi_1$ ,  $\xi_2$  and  $\tau$  in terms of the shear amount  $\omega$ , strong coupling complexities need to be treated in resolving Eq. (49) with Eqs. (50, 51). Except for simple models, results are obtained by means of numerical approximations. With a new technique in a most recent study [20], exact results are obtainable from the new model. Below are the main procedures and the main results.

First, the difference of the first two equations in Eq. (49), viz.,

$$A_{11} - A_{22} = 0$$

yields

$$\xi_2^2 = \omega^2 + \xi_1^2. \quad (52)$$

Next, the difference of the last two equations in Eq. (44), namely,

$$A_{22} - A_{33} = 0$$

produces

$$j_2^2 (z_1 + z_2) \frac{\partial W}{\partial \psi} - 3(z_1 - z_2)^2 (j_2 + 3z_1 z_2) \frac{\partial W}{\partial \gamma} = 0. \quad (53)$$

The two eigenvalues  $\chi_1$  and  $\chi_2$  in Eq. (44) are recast in the forms:

$$\chi_1 = \xi_1^2 + \omega^2 + \omega\sqrt{\xi_1^2 + \omega^2}, \quad \chi_2 = \xi_1^2 + \omega^2 - \omega\sqrt{\xi_1^2 + \omega^2}. \quad (54)$$

From Eqs. (51, 54), it may be clear that, for each value of the shear amount  $\omega$ , the solution to the averaged radius ratio  $\xi_1$  may be obtained by resolving Eq. (53), namely,

$$\xi_1 = \xi_1(\omega). \quad (55)$$

Then, solutions to  $\xi_2$  and  $\xi_3$  are obtained from Eqs. (52, 40) and given by

$$\xi_2 = \xi_2(\omega) = \sqrt{\xi_1^2 + \omega^2}, \quad (56)$$

$$\xi_3 = \xi_3(\omega) = \frac{1}{\xi_1\sqrt{\xi_1^2 + \omega^2}}. \quad (57)$$

Moreover, by using Eq. (49)<sub>4</sub> and Eq. (50)<sub>2</sub>, the solution to the shear stress may be derived as follows:

$$\tau = \tau(\omega) = \frac{1}{6}\psi^{-1}(\ln \chi_1 - \ln \chi_2) \left( 1 + 3 \left( \frac{\ln \chi_1 + \ln \chi_2}{\ln \chi_1 - \ln \chi_2} \right)^2 \right) \frac{\partial W}{\partial \psi}. \quad (58)$$

Finally, by using Eqs. (43, 58), the dimensionless twisting moment is obtained below:

$$N = N(\omega) = \frac{M}{2\pi r_0^2 t_0 E} = \frac{\xi_1}{\sqrt{\xi_1^2 + \omega^2}} \frac{\tau}{E}. \quad (59)$$

## 5 Model validation with comparison

Toward validating the new model with comparison to a few known models, numerical results will be presented with Treloar's classic data [33] for sulfur rubber and recent data [34] for soft polymer gel, separately. With the new model, such data sets for the three benchmark modes will be matched independently with the four stress–strain functions in Eqs. (31)–(35). Simulation results will be compared with those derived from the Arruda–Boyce model [6] and the Ogden model [5]. Moreover, given values of the shear amount  $\omega$ , results for a freely twisted tube will be obtained from Eq. (53) for the averaged radius ratio  $\xi_1$  and then from Eqs. (56)–(59) for the axial length ratio  $\xi_2$ , the thickness ratio  $\xi_3$  and the shear stress  $\tau$ , as well as the dimensionless twisting moment  $N$ , separately.

### 5.1 Benchmark data for sulfur rubber

We first take Treloar's data [33] for sulfur rubber into consideration. With the following parameter values:

$$\begin{aligned} E &= 1.1 \text{ MPa}, \quad \alpha = 2.3, \quad h_t = \ln 8.8, \quad h_c = \ln 44, \\ \alpha_p &= 3.4, \quad h_p = \ln 11, \quad \bar{\alpha}_p = 5.2, \quad \bar{h}_p = \ln 18, \end{aligned}$$

the stress–strain curves for the three benchmark modes are calculated from Eqs. (31)–(35) and depicted in Fig. 3. Moreover, results from the Arruda–Boyce model and the Ogden model are also calculated and incorporated in Fig. 3 for comparison. Parameter values for these two models are as follows:

$$\alpha_1 = 1.3, \quad \mu_1 = 6.3 \text{ MPa}; \quad \alpha_2 = 5.0, \quad \mu_2 = 0.012 \text{ MPa}; \quad \alpha_3 = -2.0, \quad \mu_3 = -0.1 \text{ MPa},$$

for the Ogden model (cf., Eq. (28)), and

$$Nk\theta = 0.27 \text{ MPa}, \quad n = 26.5,$$

for the Arruda–Boyce model [6]

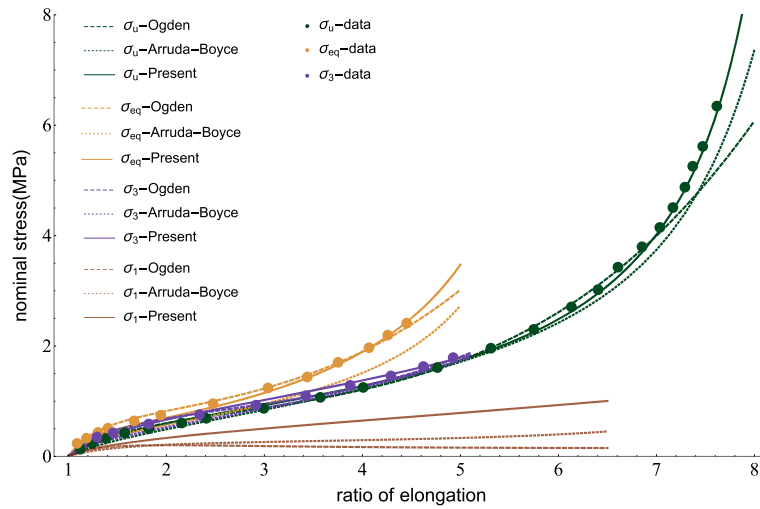


**Fig. 3** Comparison of three models in matching Treloar's data [33]

As evidenced in Fig. 3, the Ogden model agrees well with all data for the uniaxial tensile stress  $\sigma_u$ , the equi-biaxial tensile stress  $\sigma_{eq}$  and the plane-strain tensile stress  $\sigma_3$  in the loading direction, except for a few uniaxial tension data for very large stretches exceeding 7.2.<sup>2</sup> On the other side, the Arruda–Boyce model agrees well with the uniaxial and plane-strain data until large stretch, but would deviate from the bi-axial tension data from moderate to large stretches and that would also be the case for uniaxial tension data for large stretches exceeding 6.4.

The new model agrees well with all data for three benchmark modes. Also, comparison of model predictions is shown for the constrained stress in the plane-strain extension. Here, no data for the constrained stress  $\sigma_1$  in the plane-strain case are available. This stress is underestimated by both the Ogden model and the Arruda–Boyce model, as shown in Fig. 3. Further comparison with complete data will be made in the next subsection.

## 5.2 Benchmark data for PAAm-CG-6 gel

No data for the constrained stress response in the plane-strain extension case are available in Treloar's data. Recently, Yohsuke et al. [34] have performed experiments for polymer gels and supplied complete data for the three benchmark modes. Here, the data for PAAm-CG-6 gel are simulated.

With the parameter values:

$$E = 17 \text{ kPa}, \quad \alpha = 1.8, \quad h_t = \ln 6.56, \quad h_c = \ln 21, \quad \alpha_p = 3, \quad h_p = \ln 9.5, \\ \bar{\alpha}_p = 8.5, \quad \bar{h}_p = \ln 23,$$

again the stress–strain curves for the three benchmark modes are calculated from Eqs. (31)–(35) and depicted in Fig. 4. As before, results from the Arruda–Boyce model and the Ogden model are also incorporated in Fig. 4 for comparisons. Parameter values for these models as follows:

$$\alpha_1 = 1.9, \quad \mu_1 = 5 \text{ kPa}; \quad \alpha_2 = 4, \quad \mu_2 = 0.09 \text{ kPa}; \quad \alpha_3 = -2.35, \quad \mu_3 = -0.2 \text{ kPa},$$

for the Ogden model (cf., Eq. (28)), and

$$Nk\theta = 4.8 \text{ kPa}, \quad n = 20,$$

for the Arruda–Boyce model [6].

As shown in Fig. 4, the new model agrees well with all data for the three benchmark modes. Both the Ogden model and the Arruda–Boyce model agree well with the data for uniaxial and plane-strain extension. On the other hand, the Ogden model agrees approximately with the bi-axial data, while the Arruda–Boyce model would appreciably deviate from these data. In particular, either the Arruda–Boyce model or the Ogden model would lead to appreciable deviations from the data for the constrained stress  $\sigma_1$ .

<sup>2</sup> Usually, such data in Treloar [33] are not simulated for the sake of clarity.

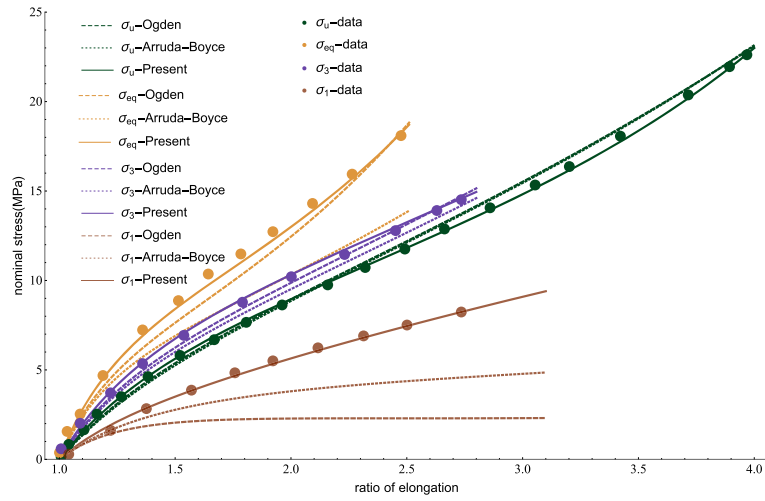


Fig. 4 Comparison of three models in matching PAAm-CG-6 gel data [34]

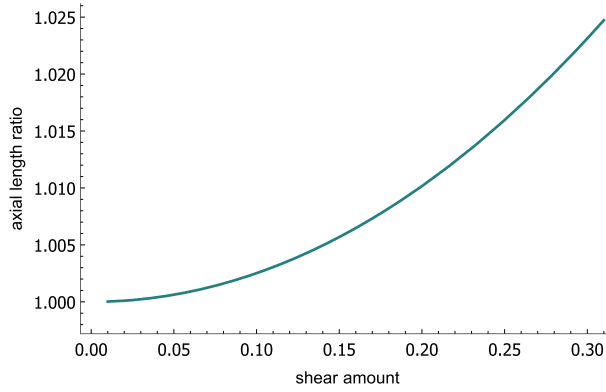


Fig. 5 Axial length ratio  $\xi_2$  in free torsion with PAAm-CG-6 gel data in [34]

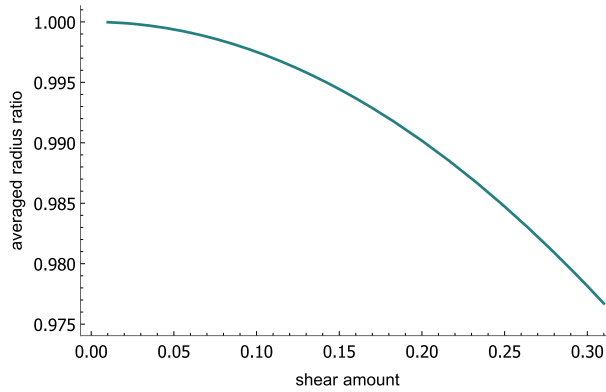
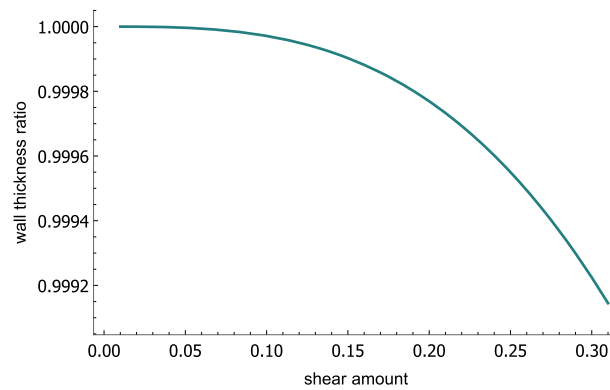


Fig. 6 Averaged radius ratio  $\xi_1$  in free torsion with PAAm-CG-6 gel data in [34]

### 5.3 Predictions for large free torsion

With test data in [34], model predictions for a freely twisted tube made of PAAm-CG-6 gel are calculated from Eqs. (53)–(59). Results are obtained in terms of the shear amount  $\omega$  and depicted in Figs. 5, 6, 7, 8, 9 for the axial length ratio  $\xi_2$ , the averaged radius ratio  $\xi_1$ , the thickness ratio  $\xi_3$ , the shear stress  $\tau$  and the dimensionless twisting moment  $N$ , separately.



**Fig. 7** Thickness ratio  $\xi_1$  in free torsion with PAAm-CG-6 gel data in [34]

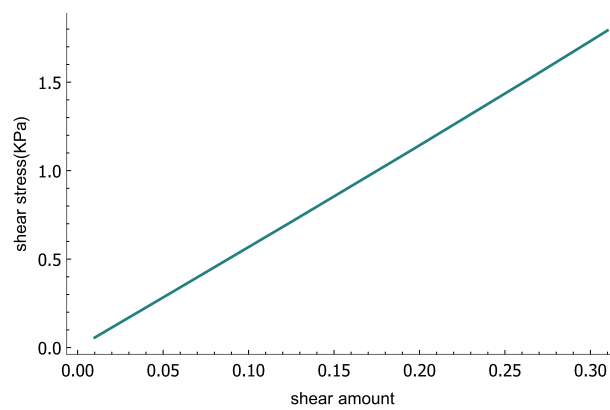


**Fig. 8** Shear stress  $\tau$  in free torsion with PAAm-CG-6 gel data in [34]

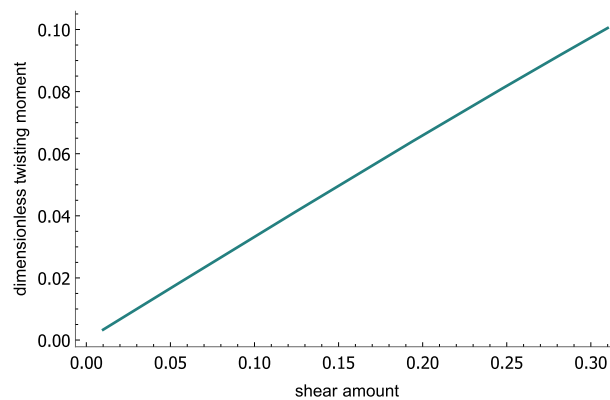


**Fig. 9** Dimensionless twisting moment  $N$  in free torsion with PAAm-CG-6 gel data in [34]

In a course of free torsion with increasing shear amount  $\omega$ , the tube is lengthening with the length ratio  $\xi_2$  increasing and becomes slender and thinner with both the averaged radius ratio  $\xi_1$  and the thickness ratio  $\xi_3$  decreasing, and, moreover, both the shear stress  $\tau$  and the dimensionless twisting moment  $N$  monotonically increases.

## 6 Concluding remarks

With two well-designed invariants representing the magnitude and the mode of the Hencky strain, a new hyper-elastic constitutive model for isotropic, incompressible elastic soft materials has been established with a new

form of the elastic potential. Exact closed-form solutions to the stress responses for three benchmark modes have been obtained in terms of four mutually independent single-variable functions. With these solutions, large strain data for three benchmark modes can be accurately and independently matched without involving usual complexities in identifying a strongly coupled set of unknown parameters. The new model has been used in an exact large strain analysis for free torsion of elastic thin-walled tubes. Numerical examples for both sulfur rubber and soft polymer gels have been presented for the purpose of model validation.

A parameter-free smooth interpolating technique (cf., e.g., [32,35,36]) may be used for the purpose of automatically and accurately matching large strain data. Moreover, the constrained torsion of thin-walled cylindrical tubes with fixed ends needs to be treated by developing the procedures in Sect. 4. Generally, large constrained and free torsion need to be studied for thin-walled tubes with composite sections.

**Acknowledgements** This study was carried out under the joint support of the fund (No. 12172149, No. 12172151) from the National Natural Science Foundation of China and the fund (No. G20221990122) from the Ministry of Science and Technology of China as well as the start-up fund from Jinan University (Guangzhou, China).

**Open Access** This article is licensed under a Creative Commons Attribution 4.0 International License, which permits use, sharing, adaptation, distribution and reproduction in any medium or format, as long as you give appropriate credit to the original author(s) and the source, provide a link to the Creative Commons licence, and indicate if changes were made. The images or other third party material in this article are included in the article's Creative Commons licence, unless indicated otherwise in a credit line to the material. If material is not included in the article's Creative Commons licence and your intended use is not permitted by statutory regulation or exceeds the permitted use, you will need to obtain permission directly from the copyright holder. To view a copy of this licence, visit <http://creativecommons.org/licenses/by/4.0/>.

**Funding** Open Access funding enabled and organized by Projekt DEAL.

## References

- Majidi, C.: Soft-matter engineering for soft robotics. *Adv. Mater. Technol.* **4**(2), 1800477 (2019)
- Hencky, H.: Über die Form des Elastizitätsgesetzes bei ideal elastischen Stoffen. *Zeit. Tech. Phys.* **9**, 215–220 (1928)
- Hencky, H.: The law of elasticity for isotropic and quasi-isotropic substances by finite deformations. *J. Rheol.* **2**(2), 169–176 (1931)
- Rivlin, R.S.: Large elastic deformations of isotropic materials III. Some simple problems in cylindrical polar co-ordinates. *Philos. Trans. R. Soc. Lond.* **A240**(823), 509–525 (1948)
- Ogden, R.W.: Large deformation isotropic elasticity—on the correlation of theory and experiment for incompressible rubberlike solids. *Proc. R. Soc.* **A326**(1567), 565–584 (1972)
- Arruda, E.M., Boyce, M.C.: A three-dimensional constitutive model for the large stretch behavior of rubber elastic materials. *J. Mech. Phys. Solids* **41**(2), 389–412 (1993)
- Gent, A.N.: A new constitutive relation for rubber. *Rubber Chem. Technol.* **69**(1), 59–61 (1996)
- Yeoh, O.H., Fleming, P.D.: A new attempt to reconcile the statistical and phenomenological theories of rubber elasticity. *J. Polym. Sci. Part B Polym. Phys.* **35**(12), 1919–1931 (1997)
- Zhan, L., Wang, S.Y., Qu, S.X., Steinmann, P., Xiao, R.: A new micro-macro transition for hyperelastic materials. *J. Mech. Phys. Solids* **171**, 105156 (2023)
- Poynting, J.H.: On pressure perpendicular to the shear planes in finite pure shears, and on the lengthening of loaded wires when twisted. *Proc. R. Soc. Lond.* **A82**(557), 546–559 (1909)
- Zubov, L.M.: Direct and inverse Poynting effects in elastic cylinders. *Dokl. Phys.* **46**, 675–677 (2001). Springer
- De Pascalis, R., Destrade, M., Saccomandi, G.: The stress field in a pulled cork and some subtle points in the semi-inverse method of nonlinear elasticity. *Proc. R. Soc.* **A463**, 2945–2959 (2007)
- Zubov, L.M., Sheidakov, D.N.: Instability of a hollow elastic cylinder under tension, torsion, and inflation. *J. Appl. Mech.* **75**, 1–6 (2008)
- Mihai, L.A., Goriely, A.: Positive or negative Poynting effect? The role of adscitious inequalities in hyperelastic materials. *Proc. R. Soc.* **A467**, 3633–3646 (2011)
- Merodio, J., Ogden, R.W.: Extension, inflation and torsion of a residually stressed circular cylindrical tube. *Contin. Mech. Thermodyn.* **28**(1), 157–174 (2016)
- Anssari-Benam, A., Horgan, C.O.: Extension and torsion of rubber-like hollow and solid circular cylinders for incompressible isotropic hyperelastic materials with limiting chain extensibility. *Eur. J. Mech. A/Solids* **92**, 104443 (2022)
- Zingerman, K.M., Zubov, L.M., Belkin, A.E., Biryukov, D.R.: Torsion of a multilayer elastic cylinder with sequential attachment of layers with multiple superposition of large deformations. *Contin. Mech. Thermodyn.* **35**(4), 1235–1244 (2023)
- Balbi, V., Trotta, A., Destrade, M., Annaiidh, A.N.: Poynting effect of brain matter in torsion. *Soft Matter*. **15**(25), 5147–5153 (2019)
- Horgan, C.O., Murphy, J.: The effect of fiber-matrix interaction on the Poynting effect for torsion of fibrous soft biomaterials. *J. Mech. Behav. Biomed. Mater.* **118**, 104410 (2021)
- Han, M.L., Wang, H.Y., Wang, S.Y., Xiao, H.: Exact large strain analysis for the Poynting effect of freely twisted thin-walled tubes made of highly elastic soft materials. *Thin-Walled Struct.* **184**, 110503 (2023)
- Hill, R.: Constitutive inequalities for isotropic elastic solids under finite strain. *Proc. R. Soc. Lond.* **A314**(1519), 457–472 (1970)

22. Anand, L.: On H. Hencky's approximate strain-energy function for moderate deformations. *J. Appl. Mech.* **46**, 78–82 (1979)
23. Fitzgerald, J.E.: A tensorial Hencky measure of strain and strain rate for finite deformations. *J. Appl. Phys.* **51**(10), 5111–5115 (1980)
24. Xiao, H.: Hencky strain and Hencky model: extending history and ongoing tradition. *Multidiscip. Model. Mater. Struct.* **1**(1), 1–52 (2005)
25. Xiao, H.: An explicit, direct approach to obtaining multiaxial elastic potentials that exactly match data of four benchmark tests for rubbery materials-part 1: incompressible deformations. *Acta Mech.* **223**(9), 2039–2063 (2012)
26. Novozhilov, V.V.: *Foundations of the Nonlinear Theory of Elasticity*. Graylock Press, Rochester N.Y (1953)
27. Kolupaev, A.V.: Generalized strength criteria as functions of the stress angle. *J. Eng. Mech.* **143**(11), 04017095 (2017)
28. Altenbach, H., Kolupaev, A.V.: General forms of limit surface: Application for isotropic materials. In: Altenbach, H. et al. (eds.), *Material Modeling and Structural Mechanics, Advanced Structured Materials* vol. **161**, 19–64 (Springer, Berlin, 2022)
29. Zhang, Y.Y., Li, H., Wang, X.M., Yin, Z.N., Xiao, H.: Direct determination of multi-axial elastic potentials for incompressible elastomeric solids: an accurate, explicit approach based on rational interpolation. *Contin. Mech. Thermodyn.* **26**(2), 207–220 (2014)
30. Jin, T.F., Yu, L.D., Yin, Z.N., Xiao, H.: Bounded elastic potentials for rubberlike materials with strain-stiffening effects. *ZAMM-J. Appl. Math. Mech.* **95**(11), 1230–1242 (2015)
31. Cao, J., Ding, X.F., Yin, Z.N., Xiao, H.: Large elastic deformations of soft solids up to failure: New hyperelastic models with error estimation. *Acta Mech.* **228**, 1165–1175 (2017)
32. Xiao, H., Yan, W.H., Zhan, L., Wang, S.Y.: Parameter-free strain-energy function which automatically and accurately matches benchmark test data for soft elastic solids. *Multidiscip. Model. Mater. Struct.* **18**(1), 129–141 (2022)
33. Treloar, L.G.: *The Physics of Rubber Elasticity*. Oxford University Press, Oxford (1975)
34. Yohsuke, B., Urayama, K., Takigawa, T., Ito, K.: Biaxial strain testing of extremely soft polymer gels. *Soft Matter* **7**(6), 2632–2638 (2011)
35. Xu, Z.H., Zhan, L., Wang, S.Y., Xi, H.F., Xiao, H.: An accurate and explicit approach to modeling realistic hardening-to-softening transition effects of metals. *ZAMM-J. Appl. Math. Mech.* **101**, 202000122 (2021)
36. Wang, S.Y., Zhan, L., Xi, H.F., Bruhns, O.T., Xiao, H.: Unified simulation of hardening and softening effects for metals up to failure. *Appl. Math. Mech.-Engl. Ed.* **42**(12), 1685–1702 (2021)